Society of Medical Education & Research

2023, Volume 3, Issue 1, Page No: 40-62

ISSN: 3108-4834

Archive of International Journal of Cancer and Allied Science

Coordinated Regulation of PD-L1 and MHC-I by the miR-23a/27a/24–2 Cluster Drives Immune Evasion in NSCLC

Javier Alonso Rodriguez[1]*, Paula Irene Diaz[1]

[1]Department of Radiation Oncology, Hospital Clinic de Barcelona, Barcelona, Spain.

***E-mail** ✉ j.rodriguez.hcb@outlook.com

Abstract

The molecules PD-L1 and MHC class I are central to how tumors avoid immune detection and resist therapies targeting the PD-1/PD-L1 axis. In this work, we found that higher levels of every microRNA belonging to the miR-23a/27a/24-2 group were linked to shorter patient survival, stronger immune suppression, and failure of PD-1/PD-L1 inhibitors among individuals with non-small cell lung cancer (NSCLC). When these miRNAs were overexpressed, they boosted PD-L1 by suppressing Cbl proto-oncogene B (CBLB) and reduced MHC-I by raising eukaryotic initiation factor 3B (eIF3B) through inhibition of microphthalmia-associated transcription factor (MITF). We also showed that continuous production of the miR-23a/27a/24-2 miRNAs in NSCLC depends on active Wnt/β-catenin signaling, which strengthens the attachment of transcription factor 4 (TCF4) to the cluster's promoter. Remarkably, blocking the eIF3B pathway with drugs greatly enhanced the response to PD-1/PD-L1 inhibitors in NSCLC patients, showing strong miR-23a/27a/24-2 cluster activity, primarily by restoring MHC-I without lowering the elevated PD-L1 caused by the cluster. In conclusion, our study reveals how the miR-23a/27a/24-2 miRNAs sustain their own presence and the specific ways they drive immune avoidance and treatment resistance in tumors. We further introduce an innovative treatment option for NSCLC cases with abundant miR-23a/27a/24-2 cluster miRNAs.

Keywords: Immune, MicroRNA, NSCLC, Cluster, Tumors

Introduction

Worldwide, lung cancer stands as the most widespread cancer and the top reason for cancer deaths [1]. Among lung cancers, non-small cell lung cancer (NSCLC) is the major form, making up roughly 85% of cases [2]. Even with recent progress in care, survival remains poor, as fewer than 20% of NSCLC patients live beyond five years [2, 3]. Accumulating data highlight that tumors' ability to dodge the immune system is a key driver of disease advancement and a serious barrier to effective treatment [4]. As a result, immune checkpoint inhibitors have gained prominence as valuable therapies for many cancers, including NSCLC, with notable success in some patients [3, 5]. Still, durable benefits are limited to only a minority, whether checkpoint blockade is used alone or paired with chemotherapy [3, 6]. Gaining a better grasp of immune escape mechanisms and reasons for treatment failure is therefore vital for advancing future care.

Various elements, especially microRNAs (miRNAs), help tumors evade immune attack. miRNA clusters are especially potent because their members can jointly influence one gene or multiple steps in the same pathway [7, 8]. The miR-23a/27a/24-2 cluster consists of miR-23a, miR-27a, and miR-24-2. Our prior research indicated these miRNAs rise early in NSCLC and trigger recurrence after surgery by stimulating Wnt/β-catenin activity [9]. Activation of this pathway has also been tied to reduced immune infiltration and poor response to checkpoint inhibitors in NSCLC [10]. Additionally, evidence suggests the cluster can block interferon-γ release and impair CD8+ T cell killing function [11]. Together, these clues suggest that elevated miR-

Access this article online https://smerpub.com/

Received: 14 October 2022; **Accepted:** 19 January 2023

How to cite this article: Rodriguez JA, Diaz PI. Coordinated Regulation of PD-L1 and MHC-I by the miR-23a/27a/24–2 Cluster Drives Immune Evasion in NSCLC Arch Int J Cancer Allied Sci. 2023;3(1):40-62. https://doi.org/10.51847/ELseCC2OGZ

23a/27a/24-2 miRNAs likely play a role in immune escape and checkpoint blockade resistance in NSCLC.

In the present investigation, we confirmed that increased miR-23a/27a/24-2 cluster miRNAs strongly correlate with immune evasion and lack of response to PD-1/PD-L1 blockade in NSCLC. These miRNAs markedly decreased interferon-γ production by T cells, reduced CD8+ T cell presence in tumors, lowered MHC class I surface levels, and raised PD-L1 expression on NSCLC cells. On a molecular level, the cluster promotes PD-L1 by inhibiting its suppressor Cbl proto-oncogene B (CBLB) and lowers MHC-I by increasing eIF3B through repression of microphthalmia transcription factor (MITF). We further discovered that Wnt/β-catenin signaling maintains the cluster's expression by enhancing TCF4 binding to its promoter. Finally, we showed that drugs targeting eIF3B or the β-catenin/TCF4 interaction improve PD-1/PD-L1 blockade outcomes in NSCLC with high cluster miRNA levels, with eIF3B inhibition offering the strongest benefit.

Materials and Methods

Human samples and cell culture

Peripheral blood samples from 20 healthy individuals were used to obtain peripheral blood mononuclear cells (PBMCs). NSCLC tissue was collected from 82 patients during surgical procedures or biopsies **(Table 1)** at Daping Hospital, with approval from the relevant ethics boards. All cell lines in this study came from the Shanghai Cell Bank of the Chinese Academy of Sciences (Shanghai, China). 293T and Lewis lung cancer (LLC) cells were grown in Dulbecco's modified Eagle's medium plus 10% fetal bovine serum (FBS) (HyClone, Logan, UT). H1299 and H1650 cells were maintained in RPMI1640 medium containing 10% FBS.

Constructs

Vectors expressing MITF (EX-B5124-M35), CBLB (EX-Z7996-M35), eIF3B shRNA (HSH066232), and matching empty or scrambled controls were bought from iGene Biotechnology Co., Ltd. (Guangzhou, China). A β-catenin expression plasmid (HG11279-CF) was sourced from Sino Biological Inc. (Beijing, China). Constructs carrying the miR-23a/27a/24-2 cluster, shRNAs, or scrambled sequences were obtained from Genechem Co. Ltd. (Shanghai, China). For luciferase assays targeting miRNAs, the 3′-untranslated regions of CBLB and MITF were PCR-amplified from normal human lung cDNA and ligated into the MluI and HindIII sites of the pMIR-REPORT™ vector (Thermo Fisher Scientific, Waltham, MA, USA). For promoter studies, the miR-23a/27a/24-2 promoter sequence was amplified from human genomic DNA and cloned into the NheI and BglII sites of the pGL4.10 vector (Promega, Madison, WI, USA).

Co-culturing of T cells with tumor cells

Peripheral blood mononuclear cells (PBMCs) were separated from whole blood samples obtained from healthy volunteers using lymphocyte separation medium, following the protocol provided by the manufacturer (Tian Jin Hao Yang Biological Manufacture Co., Ltd, Tianjin, China). Immune cells were subsequently stimulated according to an established method [12]. CD8+ T cells were then purified with a CD8+ T cell isolation kit (Miltenyi Biotec) as per the supplied guidelines.

Assessment of T cell-mediated tumor cell killing was conducted following a previously reported procedure [12]. In brief, non-small cell lung cancer (NSCLC) cells were transfected with either an empty vector or constructs overexpressing the miR-23a/27a/24−2 cluster. Forty-eight hours post-transfection, the NSCLC cells were incubated with activated T cells at a 1:20 target-to-effector ratio for 6 hours, after which cell viability loss was quantified via flow cytometry.

The migration of CD8+ T cells was evaluated using a protocol outlined by Shang *et al*. [13]. Concisely, NSCLC cells received transfection with a control vector or a miR-23a/27a/24−2 cluster overexpression plasmid, followed by medium replacement 48 hours later. After an additional 48 hours in fresh medium, the conditioned supernatant was placed in the lower compartment of a Transwell system. Meanwhile, 5 × 10^5 activated CD8+ T cells, pre-labeled with anti-human CD8α APC-Cy7 antibody (Invitrogen, Cat#: A15448), were suspended in 100 μL medium and added to the upper chamber. Following a 2-hour incubation period, the number of T cells that had migrated was determined by flow cytometry.

To examine how overexpression of the miR-23a/27a/24−2 cluster in NSCLC cells influences interferon-gamma (IFN-γ) release from T cells, NSCLC cells were transfected with the specified plasmids. At 48 hours after transfection, these cells were co-incubated with activated T cells at a 1:10 ratio for 12 hours. The supernatant was then harvested, and IFN-γ levels were

determined using a human IFN-γ ELISA kit (Invitrogen) in accordance with the manufacturer's directions.

Luciferase reporter assays

In the miRNA target reporter experiments, 293T cells were co-transfected with either miR-23a/27a/24−2 cluster expression plasmids or control vectors alongside firefly luciferase reporters harboring the 3′-UTR of CBLB or MITF. For analysis of the miR-23a/27a/24−2 cluster promoter, 293T cells received TCF4 or β-catenin expression constructs (or empty vectors) together with firefly luciferase reporters containing the cluster promoter region. A Renilla luciferase plasmid was included in all transfections as an internal normalization control. Seventy-two hours post-transfection, cells were collected, and luciferase activities were assessed using the Dual-Luciferase Reporter Assay System (Promega).

Western Blotting (WB), Immunohistochemistry (IHC), Immunofluorescence (IF), and Co-Immunoprecipitation (Co-IP) analyses

These techniques—WB, IHC, IF, and Co-IP—were carried out as detailed in prior work [14]. Densitometric analysis of WB bands was performed using ImageJ software. IHC staining intensity was evaluated blindly by two independent pathologists unaware of clinical data. Primary antibodies specific for eIF3B (Cat No: bs-14542R, Lot No: BC12254757; IHC), MITF (Cat No: bsm-51339 M, Lot No: BD06051693), MHC-I (Cat No: bs-18070R, Lot No: BD07151765, WB; bs-2355R, Lot No: BD07151765, IHC/IF), and PD-L1 (Cat No: bs-22022R, Lot No: BD7153735, flow cytometry) were sourced from Beijing Biosynthesis Biotechnology Co., Ltd (Beijing, China). Antibodies against β-catenin (Cat No:8480 S, Lot No:5), Histone H3 (Cat No:9715 S, Lot No:20), and Actin (Cat No:4970 S, Lot No:20) were acquired from Cell Signaling Technology (Danvers, MA, USA). CD8 antibodies (Cat No: ab217344, Lot No:00121531; Cat No: ab17147, Lot No:3258634-5) and PD-L1 antibody (Cat No: ab279292, Lot No: 1007824-2, WB) were obtained from Abcam (Cambridge, MA, USA). Antibodies recognizing CBLB (Cat No: 66353-1, Lot No: 10003654), TCF4 (Cat No: 22337-1-AP, Lot No: 00121531), eIF3B (Cat No: 68202-1, Lot No: 10028876, WB), and PD-L1 (Cat No: 66248-1, Lot No: 10022147, IHC) were supplied by Proteintech (Wuhan, Hubei, China). Control rabbit IgG (Cat No:30000-0-AP, Lot No: 00140749) and mouse IgG (Cat No: BS-0296P, Lot No: BC06261797) were provided by Proteintech and Beijing Biosynthesis Biotechnology Co., Ltd, respectively.

Quantitative real-time reverse transcription PCR (qRT-PCR) and miRNA In Situ Hybridization (ISH)

Total RNA was extracted with TRIzol reagent (Beyotime, Shanghai, China). Gene mRNA levels were quantified by qRT-PCR employing the SYBR Green One-Step qRT-PCR kit (Beyotime Biotechnology) per the provided protocol. Primers for U6, hsa-miR-23a, hsa-miR-24-2, and hsa-miR-27a were obtained from GeneCopoeia (Rockville, MD, USA), and miRNA expression was measured using the All-in-One™ miRNA qRT-PCR Detection Kit 2.0 (GeneCopoeia) following manufacturer guidelines. miRNA expression values were normalized relative to U6.

In situ hybridization for miRNAs and subsequent scoring were executed according to the methods described by Nuovo [15] and Guo *et al*. [16], respectively. In short, paraffin-embedded sections underwent deparaffinization, followed by antigen retrieval through 15-minute boiling in citric acid buffer. Sections were digested with proteinase K for 15 minutes and then incubated with pre-hybridization buffer for 1 hour at 37°C. Hybridization was performed overnight at 37°C using a buffer containing probes for miR-23a, miR-24-2, or miR-27a (or no probe as a negative control). All miRNA probes for ISH were custom-synthesized by Zoonbio Biotechnology Co., Ltd (Nanjing, China).

RNA sequencing and proteomics analysis

Transcriptome sequencing and subsequent data processing were carried out by Shanghai Genechem Co., Ltd, following the methodology outlined by Li *et al*. [17]. In short, Illumina-compatible RNA libraries were prepared using the NEBNext Ultra RNA Library Prep Kit, followed by sequencing on the Illumina NovaSeq platform. Raw FASTQ files were handled with custom Perl scripts, and alignment was performed using Hisat2, which generated a splice junction database based on the provided gene annotation model.

Proteomic profiling was conducted according to an earlier-described protocol [18]. Concisely, H1299 cells received transfection with either the miR-23a/27a/24−2 cluster overexpression construct or control vector. Seventy-two hours later, cellular proteins were isolated, denatured, enzymatically digested, and tagged with iTRAQ reagents. Peptides were then separated by high-performance liquid chromatography on an Agilent 1260

Infinity II system. Mass spectrometric acquisition was achieved using a Q-Exactive Plus instrument (Thermo Fisher Scientific) interfaced with an Easy-nLC system (Thermo Fisher Scientific). Dataset interpretation was performed with Mascot version 2.6 and Proteome Discoverer 2.1.

Electrophoretic Mobility Shift Assay (EMSA)

Potential TCF4 binding sites within the miR-23a/27a/24−2 cluster were identified through the hTFtarget database [19]. The EMSA procedure was executed with the LightShift Chemiluminescent Kit (Thermo Fisher Scientific), adhering to the manufacturer's guidelines and as previously detailed [14].

Chromatin Immunoprecipitation (ChIP)-qPCR Assay

For ChIP-qPCR experiments, 293T cells were transfected with a β-catenin expression plasmid or an empty vector. At 48 hours post-transfection, cells were fixed with 1% formaldehyde at room temperature, and the reaction was quenched by adding glycine. Cells were subsequently lysed in ChIP buffer, fragmented by sonication, precleared, and incubated overnight with 2 µg of anti-TCF4 antibody or control IgG, followed by precipitation using protein G/A agarose beads. Beads underwent sequential washes with low- and high-salt buffers, and bound complexes were released by incubation in elution buffer at 65°C for 15 minutes. After centrifugation to recover the supernatant, samples were supplemented with NaCl (final concentration 0.2 M) and incubated overnight at 65°C for reverse crosslinking. Purified DNA was then analyzed by quantitative PCR.

In vivo studies

Six-week-old female C57BL/6J mice and male SCID mice (Beijing HFK Bioscience Co., Ltd, Beijing, China) were employed in the animal experiments. The role of the miR-23a/27a/24−2 cluster in promoting immune escape in lung cancer was assessed using C57BL/6J and SCID xenograft models. To establish the C57BL/6J model, 1 × 10^6 LLC cells transfected with a control vector, miR-23a/27a/24−2 cluster overexpression plasmid, scramble control, or shRNA targeting the cluster were suspended in 100 µL PBS and injected subcutaneously into the flank. For the SCID model, 2 × 10^6 H1299 cells transfected with a scramble or shRNA-expressing plasmid against the miR-23a/27a/24−2 cluster in 100 µL PBS were implanted subcutaneously. Three days after tumor cell inoculation, mice received either no treatment or 3 × 10^6 human PBMCs via tail vein injection. Tumor dimensions were recorded weekly.

The contribution of the miR-23a/27a/24−2 cluster to resistance against PD-1/PD-L1 blockade was evaluated in C57BL/6J xenografts. Mice were subcutaneously implanted with 1 × 10^6 LLC cells transfected with empty vector or miR-23a/27a/24−2 cluster plasmid in 100 µL PBS. Once tumors reached approximately 100 mm^3, animals were administered either anti-PD-L1 monoclonal antibody (1 mg/kg body weight) or control rat IgG (Bio X cell) intravenously every three days **(Figure 1a).**

To assess the combined therapeutic efficacy of LF3 and PD-1/PD-L1 inhibition in tumors overexpressing the miR-23a/27a/24−2 cluster, C57BL/6J xenografts were established with high-expressing LLC cells as described. When tumors attained ~100 mm^3, mice were randomized into four groups: control (IgG), anti-PD-L1 mAb alone (1 mg/kg every three days), LF3 alone (50 mg/kg every two days), or the combination of both agents, all delivered intravenously **(Figure 1b).**

The comparative impact of LF3 versus 4EGI-1 on enhancing PD-1/PD-L1 blockade was examined similarly in C57BL/6J models with high miR-23a/27a/24−2 cluster-expressing LLC cells. Upon tumors reaching ~100 mm^3, mice were divided into three groups receiving anti-PD-L1 mAb alone (1 mg/kg every three days), anti-PD-L1 plus LF3, or anti-PD-L1 plus 4EGI-1 (75 mg/kg intraperitoneally, 5 days per week) **(Figure 1c).** All procedures involving animals were conducted in accordance with the institutional guidelines of the Army Medical University on laboratory animal welfare.

Statistical analysis

Results are expressed as mean ± standard deviation from at least three independent replicates. Statistical comparisons were performed using SPSS software, with differences deemed significant at $p < 0.05$.

Results and Discussion

Elevated levels of miRNAs in the miR-23a/27a/24−2 cluster are closely linked to tumor progression and immune escape in NSCLC

To examine the relationship between miRNA expression in the miR-23a/27a/24−2 cluster and NSCLC advancement, patients exhibiting higher tumor levels of

all three miRNAs relative to paired adjacent normal tissues were classified as the high-expression group. Conversely, those with tumor levels equal to or lower than adjacent tissues for all miRNAs were assigned to the low-expression group. Clinical correlations demonstrated that increased miR-23a/27a/24−2 cluster expression was inversely associated with overall survival **(Figure 1a)** and disease-free survival **(Figure 1b)** among NSCLC patients. Moreover, the high-expression group displayed markedly reduced CD8+ T cell infiltration within tumor specimens **(Figure 1c).** Gene Ontology (GO) enrichment performed on transcriptome data from H1299 cells with silenced miR-23a/27a/24−2 cluster versus controls indicated significant impacts on T cell activation and differentiation pathways **(Figure 1d).** Gene set enrichment analysis (GSEA) further showed a negative correlation between cluster expression and T cell-mediated immune responses in NSCLC **(Figure 1e).** Supporting evidence emerged from public GEO repository analysis, where the cluster's expression similarly linked to T cell activation and differentiation **(Figure 1f).** Additionally, target prediction-based functional annotation of these miRNAs highlighted involvement in immune-related processes [20] **(Figure 1g)**. Collectively, these observations imply that overexpression of the miR-23a/27a/24−2 cluster promotes NSCLC progression through suppression of T cell antitumor immunity.

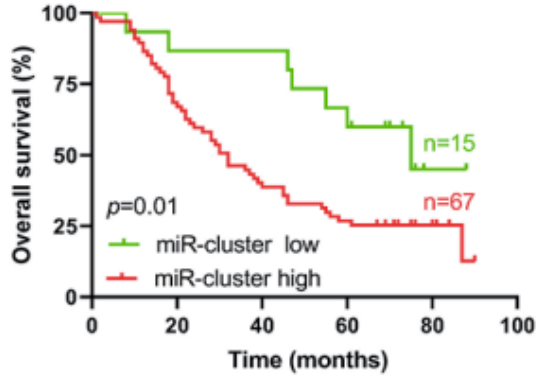

a)

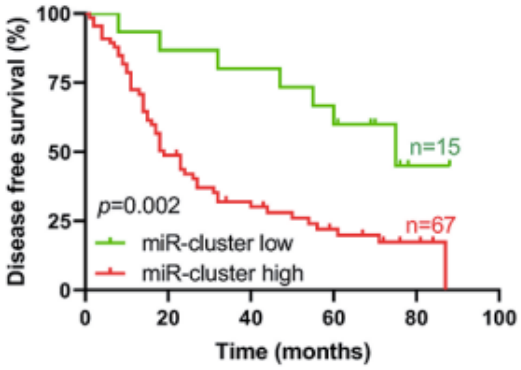

b)

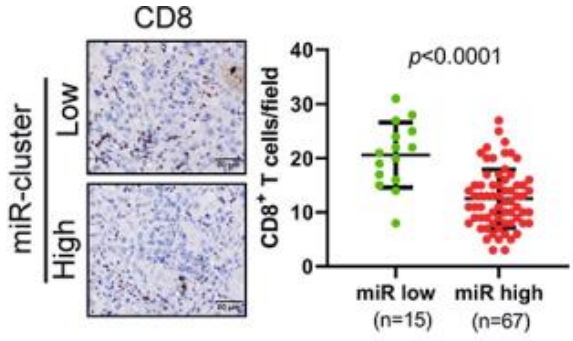

c)

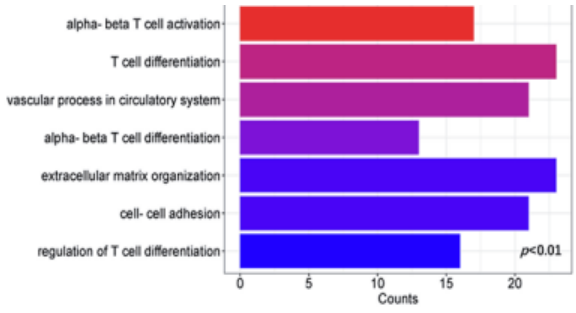

d)

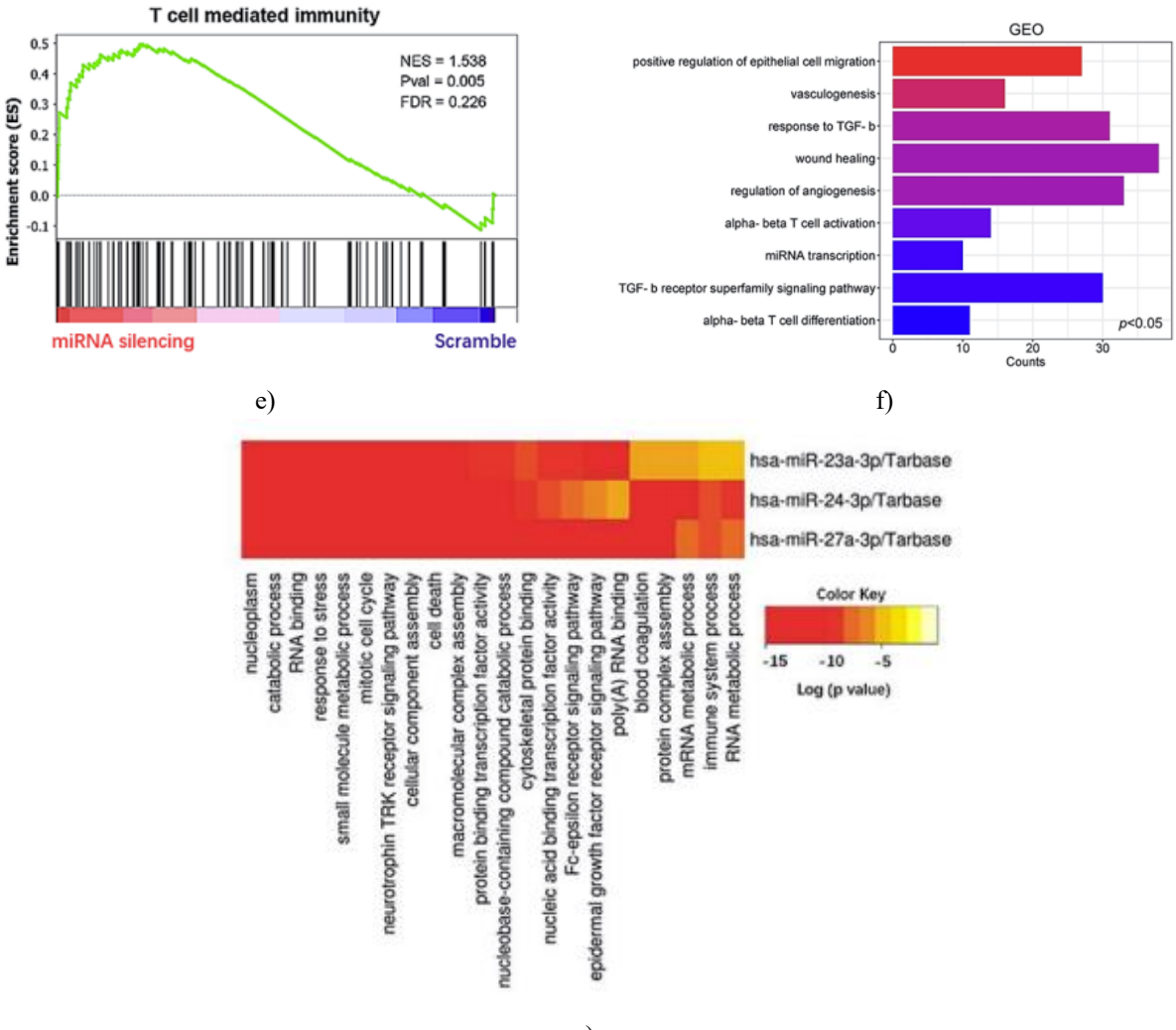

Figure 1. Elevated miR-23a/27a/24−2 cluster expression is tightly associated with unfavorable outcomes and immune evasion in NSCLC. (a) Kaplan-Meier curves illustrating reduced overall survival and (b) reduced disease-free survival in patients with high cluster expression. Analyses involved 82 NSCLC cases, with log-rank testing for significance. (c) Representative IHC staining for CD8+ T cells and quantification of infiltrates in NSCLC samples (100 × 100 μm field). Significance determined by t-test. (d) GO enrichment derived from RNA-seq of miR-23a/27a/24−2 cluster-knockdown H1299 cells versus controls. (e) GSEA demonstrates an inverse correlation between cluster expression and T cell-mediated immunity, based on the same RNA-seq dataset. (f) GO analysis conducted on the GEO dataset GSE151103. (g) Target gene-based GO analysis for the miRNAs (via http://www.microrna.gr/miRPathv4). miR-cluster, miR-23a/27a/24−2 cluster.

Overexpression of the miR-23a/27a/24−2 cluster in NSCLC suppresses T Cell Antitumor activity

To determine if NSCLC cells overexpressing the miR-23a/27a/24−2 cluster directly impair T cell responses, activated T cells were co-incubated with modified NSCLC cells **(Figure 2a),** followed by functional evaluations. Findings indicated that elevated cluster expression in tumor cells substantially decreased IFN-γ production by T cells **(Figures 2a and 3a),** diminished T cell-induced tumor cell killing **(Figures 2b and 3b)**, and hindered T cell chemotaxis **(Figures 2c 3c).** The cluster's contribution to immune evasion was further explored in vivo using Lewis lung carcinoma (LLC) models. Given that LLC tumors develop in immunocompetent C57BL/6J mice, this system is suitable for immunity studies [21]. In C57BL/6J xenografts, enforced

overexpression of the entire cluster in LLC cells (**Figure 2b)** markedly accelerated tumor expansion **(Figures 2d and 4a),** reduced CD8+ T cell tumor infiltration **(Figure 2e)**, and lowered T cell IFN-γ release **(Figure 2f).** Conversely, cluster knockdown in LLC cells **(Figure 2c)** retarded tumor growth **(Figures 2g and 4b),** enhanced CD8+ T cell presence **(Figure 2h),** and boosted IFN-γ levels **(Figure 2i).** These patterns were validated in additional models. Knockdown of the cluster in H1299 cells **(Figure 2d)** notably suppressed tumor development in SCID mice, both with **(Figures 2j and 4c)** and without **(Figures 2l and 4d)** human PBMC transfer. In PBMC-treated SCID hosts, cluster inhibition also augmented T cell infiltration **(Figure 2k).** Strikingly, adoptive PBMC transfer amplified the growth-inhibitory effect of cluster silencing **(Figure 2m).** Overall, these results underscore the miR-23a/27a/24−2 cluster's involvement in dampening T cell-driven antitumor immunity.

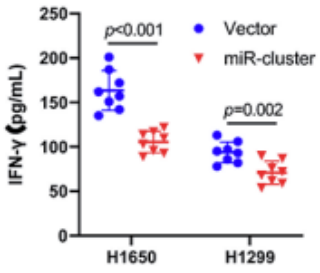

a)

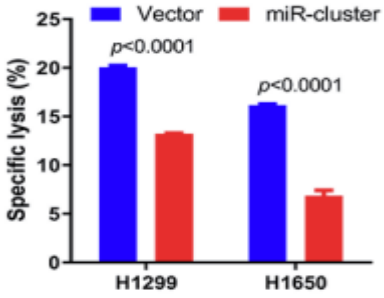

b)

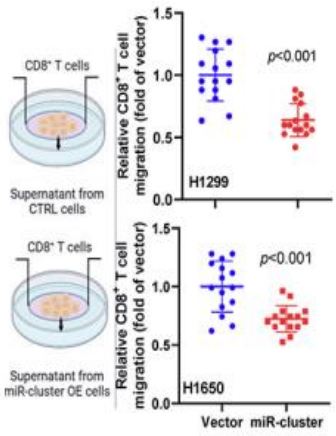

c)

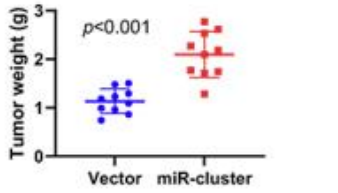

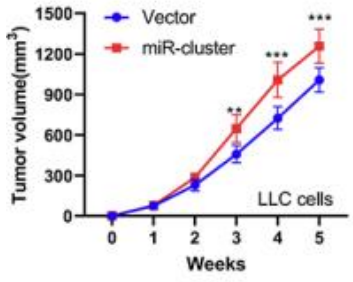

d)

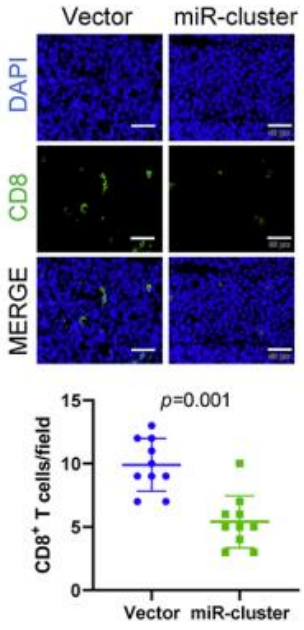

e)

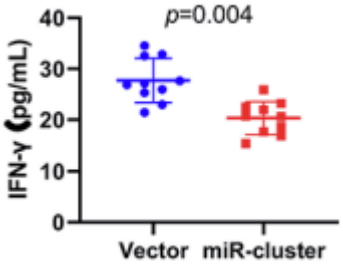

f)

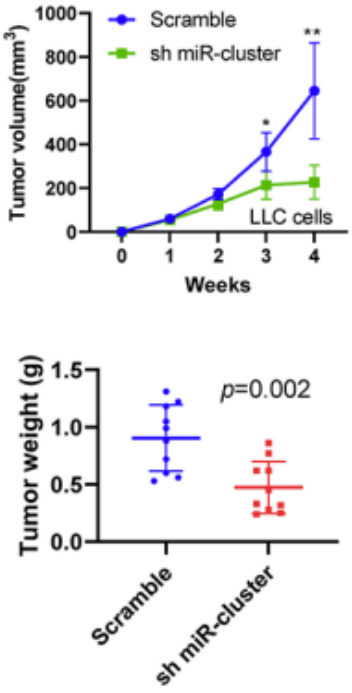
Scramble
sh miR-cluster
Tumor volume(mm3)
LLC cells
Weeks
Tumor weight (g)
p=0.002
Scramble
sh miR-cluster

g)

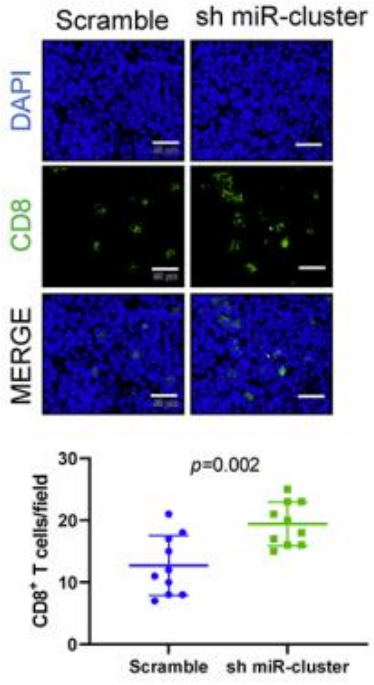
Scramble
sh miR-cluster
DAPI
CD8
MERGE
CD8+ T cells/field
p=0.002
Scramble
sh miR-cluster

h)

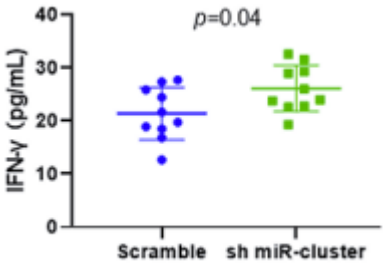
IFN-γ (pg/mL)
p=0.04
Scramble
sh miR-cluster

i)

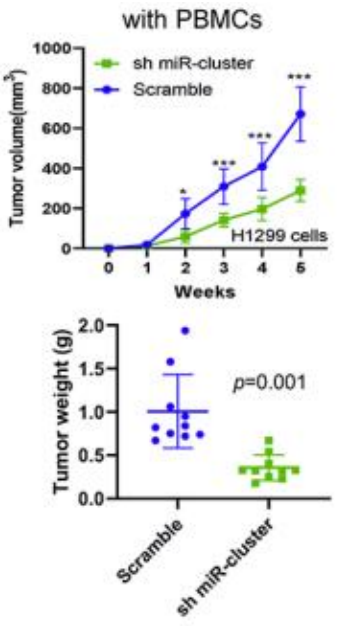
with PBMCs
sh miR-cluster
Scramble
Tumor volume(mm3)
H1299 cells
Weeks
Tumor weight (g)
p=0.001
Scramble
sh miR-cluster

j)

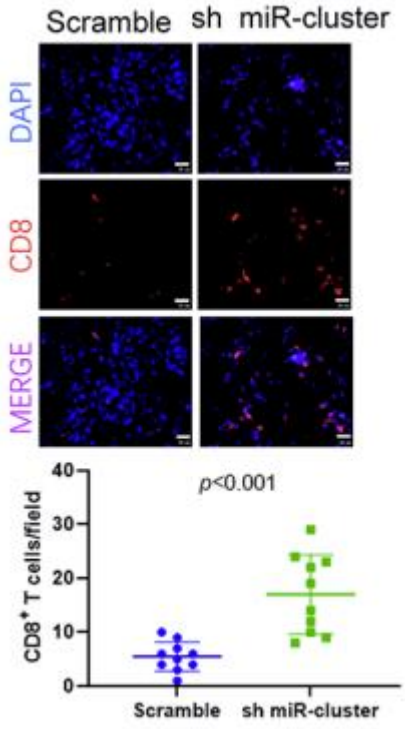
Scramble
sh miR-cluster
DAPI
CD8
MERGE
CD8+ T cells/field
p<0.001
Scramble
sh miR-cluster

k)

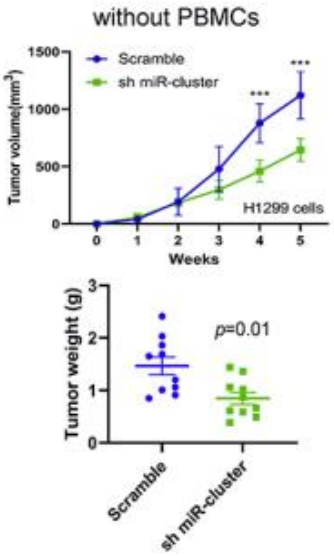
without PBMCs
Scramble
sh miR-cluster
Tumor volume(mm3)
H1299 cells
Weeks
Tumor weight (g)
p=0.01
Scramble
sh miR-cluster

l)

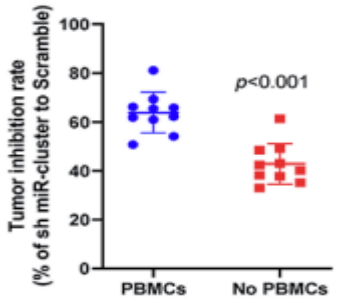

m)

Figure 2. The miR-23a/27a/24−2 cluster suppresses T cell-driven immune responses in NSCLC. (a) IFN-γ levels in supernatant following 12-hour co-culture of CD8+ T cells with NSCLC cells at a 10:1 ratio. (b) Quantification of CD8+ T cell-mediated killing of NSCLC cells via flow cytometry. NSCLC cells were transfected with a control vector or a miR-23a/27a/24−2 cluster construct, then co-incubated with activated CD8+ T cells at a 1:20 ratio for 6 hours. (c) Normalized migration of human CD8+ T cells toward conditioned medium from H1299 or H1650 cells transfected with control vectors or miR-23a/27a/24−2 cluster overexpression plasmids. (d) Tumor growth curves and final weights in subcutaneous C57BL/6J xenografts established with LLC cells transfected with control vectors or miR-23a/27a/24−2 cluster constructs. (e) Representative immunofluorescence staining for CD8+ T cells and quantification of infiltrates in xenograft tumors (100 × 100 μm field). Samples from (d) (scale bar: 50 μm); CD8+ T cells appear green. (f) IFN-γ concentrations in tumor lysates from the C57BL/6J model in (d). (g) Tumor growth curves and weights in C57BL/6J xenografts using LLC cells transfected with scramble control or shRNA targeting the miR-23a/27a/24−2 cluster. (h) Representative immunofluorescence for CD8+ T cells and infiltrate counts (100 × 100 μm field) in tumors from (g); CD8+ T cells green (scale bar: 50 μm). (i) IFN-γ levels in tumor tissues from (g). (j) Tumor growth and weights in PBMC-treated SCID xenografts generated with H1299 cells transfected with scramble or miR-23a/27a/24−2 cluster shRNA constructs. (k) Representative immunofluorescence for CD8+ T cells and infiltrate quantification (100 × 100 μm field) in SCID tumors from (j) (scale bar: 50 μm); CD8+ T cells red. (l) Tumor growth and weights in untreated SCID xenografts using H1299 cells transfected with scramble or cluster shRNA constructs. (m) Relative tumor suppression achieved by cluster knockdown in SCID models with or without PBMC administration. Data derived from (j) and (l). Animal studies included 10 mice per group. In vitro assays were performed in triplicate. Values represent mean ± SD. Significance assessed by t-test: *, $p < 0.05$; **, $p < 0.01$; ***, $p < 0.001$ versus vector or scramble control. LLC, Lewis lung carcinoma; IFN-γ, interferon-γ; miR-cluster, miR-23a/27a/24−2 cluster; sh miR-cluster, shRNA against miR-23a/27a/24−2 cluster; PBMCs, peripheral blood mononuclear cells.

miRNAs in the miR-23a/27a/24−2 cluster enhance PD-L1 and reduce MHC-I expression in NSCLC

To identify proteins mediating the immunosuppressive actions of the miR-23a/27a/24−2 cluster on T cell responses, proteomic profiling was conducted on NSCLC cells overexpressing the entire cluster versus controls. Results showed altered abundance of numerous proteins, notably upregulation of PD-L1 and downregulation of MHC-I, both critical for immune escape and resistance to immune checkpoint blockade **(Figure 3a)**. GO enrichment further linked cluster overexpression to pathways involving MHC-I antigen processing and presentation **(Figure 3a).** Western blotting confirmed elevated PD-L1 and reduced MHC-I protein levels in cluster-overexpressing cells, irrespective of IFN-γ stimulation **(Figures 3b and 5a).** This indicates direct regulation of these molecules by the cluster, independent of T cell IFN-γ reduction. Co-overexpression of all three miRNAs exerted stronger effects on PD-L1 and MHC-I than individual miRNAs **(Figure 7),** pointing to synergistic activity. Flow cytometry **(Figure 3c)** and immunofluorescence **(Figure 3d)** validated these expression changes. Proteomics findings aligned with these observations. In vivo, IHC of LLC-derived C57BL/6J xenografts revealed heightened PD-L1 and diminished MHC-I in cluster-overexpressing tumors **(Figure 3e).** Similar patterns emerged in human NSCLC specimens by IHC **(Figure 3f).** Overall, these

results support a mechanism whereby the miR-23a/27a/24−2 cluster impairs T cell antitumor activity via PD-L1 induction and MHC-I suppression in NSCLC.

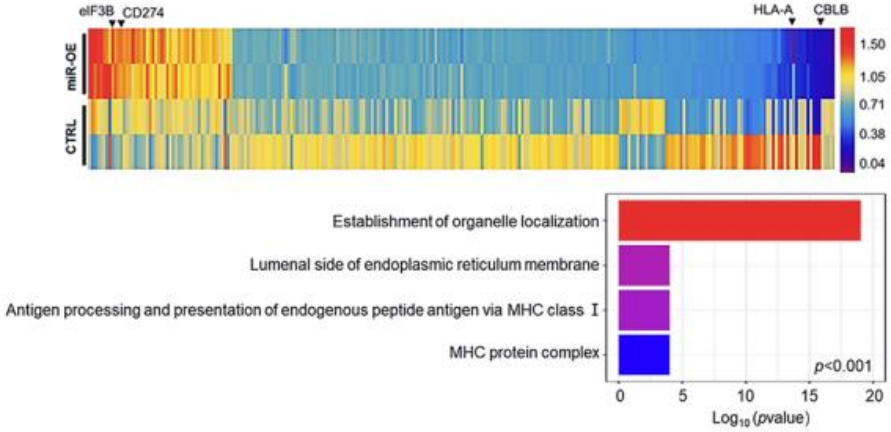

a)

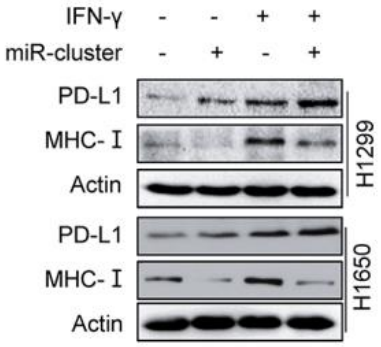

b)

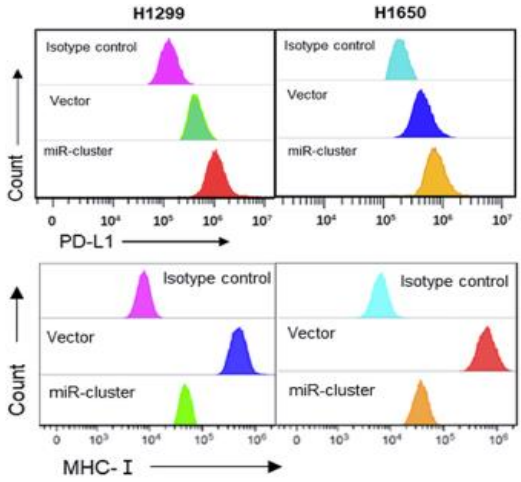

c)

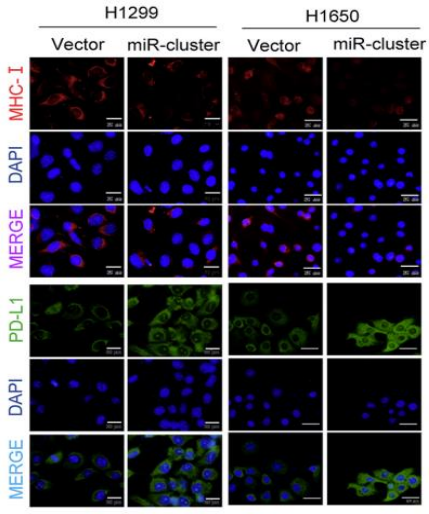

d)

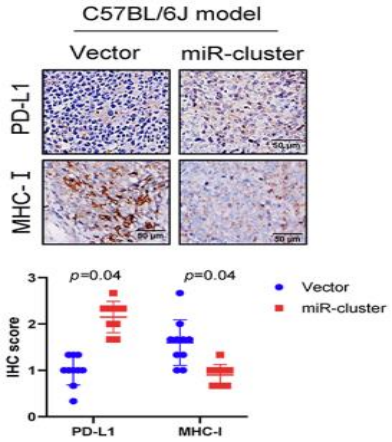

e)

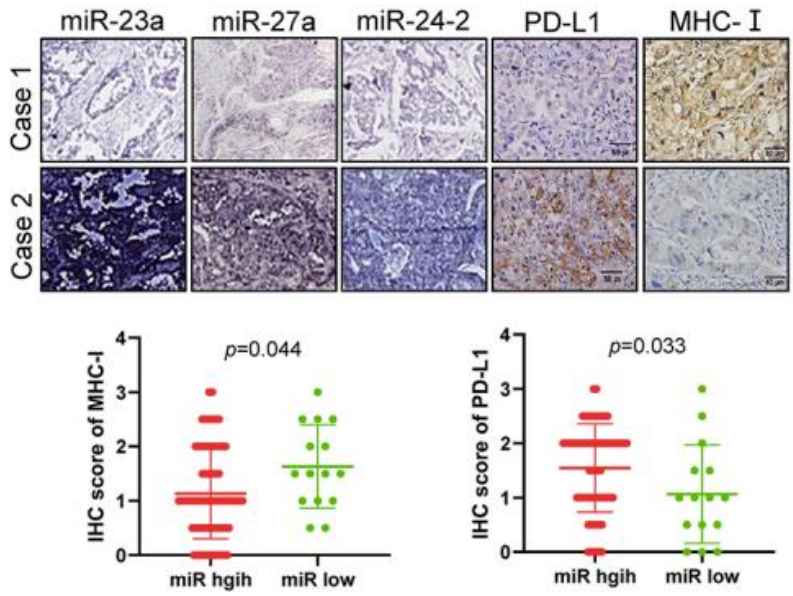

f)

Figure 3. The miR-23a/27a/24−2 cluster modulates PD-L1 and MHC-I levels in NSCLC. (a) Heatmap of differentially expressed proteins and GO enrichment based on proteomics from cluster-overexpressing H1299 cells versus controls. (b) Western blots demonstrating cluster-mediated PD-L1 upregulation and MHC-I downregulation in NSCLC cells treated with or without 20 ng/ml IFN-γ for 24 hours. (c) Flow cytometry and (d) immunofluorescence (scale bar: 20 μm) confirming MHC-I reduction and PD-L1 increase upon cluster overexpression. Cells were analyzed 72 hours post-transfection with vector or cluster construct (b-d). Experiments repeated thrice. (e) Representative IHC staining and scoring for PD-L1 and MHC-I in C57BL/6J xenografts from **Figure 2d** (scale bar: 50 μm). (f) IHC images and scores for PD-L1 and MHC-I in NSCLC patient tumors with high (n = 67) or low (n = 15) cluster expression (scale bar: 50 μm). Significance by the Wilcoxon signed-rank test (e) or the rank-sum test (f). miR-cluster, miR-23a/27a/24−2 cluster; miR-OE, cluster overexpression; CTRL, control; miR high, high cluster miRNA levels; miR low, low cluster miRNA levels.

miRNAs in the miR-23a/27a/24−2 cluster elevate PD-L1 Levels in NSCLC via CBLB suppression

To elucidate how the miR-23a/27a/24−2 cluster controls PD-L1 in NSCLC, attention turned to proteomics data showing reduced CBLB—a known PD-L1 negative regulator [22]—in overexpressing cells **(Figure 3a).** Western blot and qRT-PCR verified cluster-dependent CBLB downregulation at protein **(Figures 4a, 5b and 6)** and mRNA **(Figure 4b)** levels. Restoring CBLB expression abrogated cluster-induced PD-L1 elevation **(Figures 4c and 5c),** implicating CBLB repression as key to PD-L1 upregulation. Bioinformatic prediction (targetscan.org) identified binding sites for miR-23a and miR-27a in the CBLB 3′-UTR **(Figure 4d).** Luciferase assays demonstrated that cluster overexpression inhibited reporter activity driven by wild-type but not mutant CBLB 3′-UTR **(Figure 4e).** Inverse cluster-CBLB and direct cluster-PD-L1 correlations were corroborated by IHC in cluster-overexpressing LLC xenografts **(Figure 4f)** and human NSCLC tissues **(Figure 4g).** In summary, the miR-23a/27a/24−2 cluster promotes PD-L1 expression in NSCLC by directly targeting and inhibiting CBLB through its 3′-UTR.

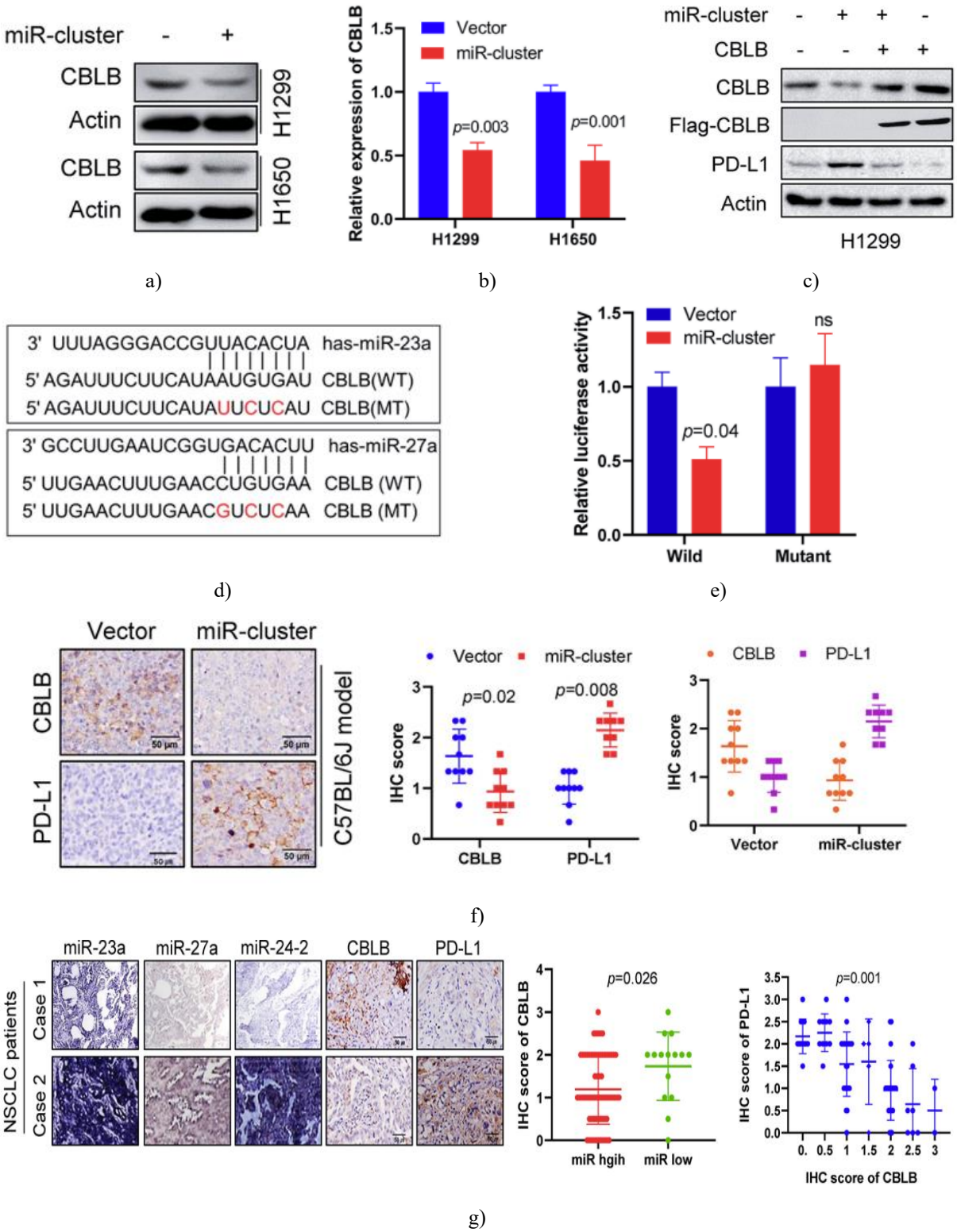

Figue 4. The miR-23a/27a/24−2 cluster enhances PD-L1 levels via direct targeting of CBLB in NSCLC. (a) Western blotting and (b) qRT-PCR demonstrating that enforced expression of the miR-23a/27a/24−2 cluster reduces CBLB at protein and mRNA levels. (c) Restoration of CBLB blocks the cluster-mediated increase in PD-L1 in H1299 cells. NSCLC cells received transfection with control vector, cluster overexpression construct,

and/or CBLB expression plasmid. Analyses performed 72 hours later. Experiments repeated thrice (a-c). (d) Alignment of sequences showing potential binding of cluster miRNAs to the CBLB 3′ UTR. (e) Luciferase reporter assays indicate that cluster overexpression inhibits activity from the wild-type CBLB 3′ UTR but not from mutated versions in NSCLC cells. (f) Representative IHC staining and scoring for CBLB and PD-L1 in C57BL/6J xenograft tumors from **Figure 2d** (scale bar: 50 μm). (g) Representative IHC images and scores for CBLB and PD-L1 in NSCLC patient samples with high (n = 67) or low (n = 15) cluster expression (scale bar: 50 μm). Values are mean ± SD. Significance determined by t-test (B and E), Wilcoxon signed-rank test (f), Wilcoxon rank-sum test (g-left), and one-way ANOVA (G-right). miR-cluster, miR-23a/27a/24−2 cluster; miR high, elevated miR-23a/27a/24−2 cluster miRNA levels; miR low, reduced miR-23a/27a/24−2 cluster miRNA levels.

miRNAs in the miR-23a/27a/24−2 cluster reduce MHC-I Levels in NSCLC via MITF suppression

The mechanism underlying cluster regulation of MHC-I was further explored. Proteomics identified increased eIF3B in cluster-overexpressing cells **(Figure 3a).** Bioinformatic predictions showed binding sites for all three cluster miRNAs in the MITF 3′-UTR **(Figure 5a).** Prior work indicates that MITF suppresses eIF3B, while eIF3B in turn represses MHC-I [23], raising the possibility that the cluster downregulates MHC-I by elevating eIF3B through MITF inhibition. Supporting this, cluster overexpression markedly decreased MITF and MHC-I while increasing eIF3B protein levels in NSCLC cells **(Figures 5b, 5d and 6).** Cluster-dependent MITF reduction was also evident at the transcript level **(Figure 5c).** Critically, MITF restoration or eIF3B knockdown rescued MHC-I expression suppressed by the cluster, and MITF overexpression prevented cluster-induced eIF3B elevation **(Figures 5d and 5e).** Luciferase assays confirmed direct targeting: cluster overexpression diminished reporter activity from wild-type MITF 3′-UTR but spared mutant constructs **(Figure 5e).** Relationships between cluster expression, MITF, eIF3B, and MHC-I were validated by IHC in cluster-overexpressing LLC xenografts **(Figure 5f)** and human NSCLC specimens **(Figrue 5g).** In summary, the miR-23a/27a/24−2 cluster suppresses MHC-I in NSCLC by promoting eIF3B via direct repression of MITF.

a)

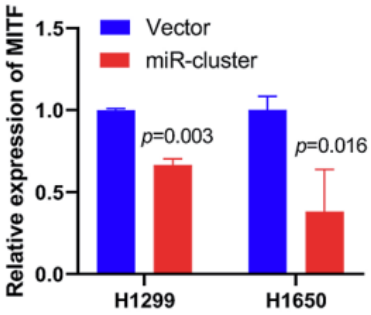

c)

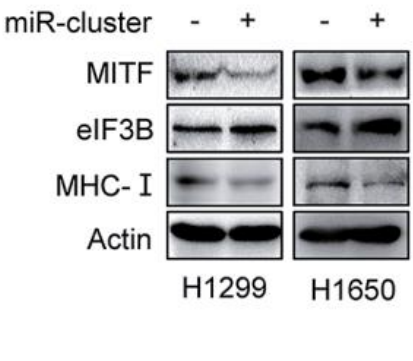

b)

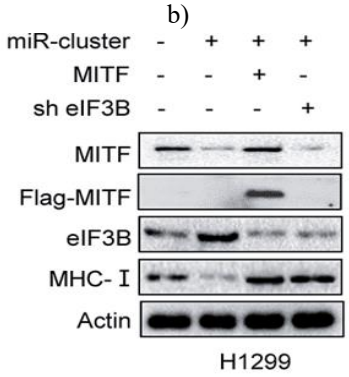

d)

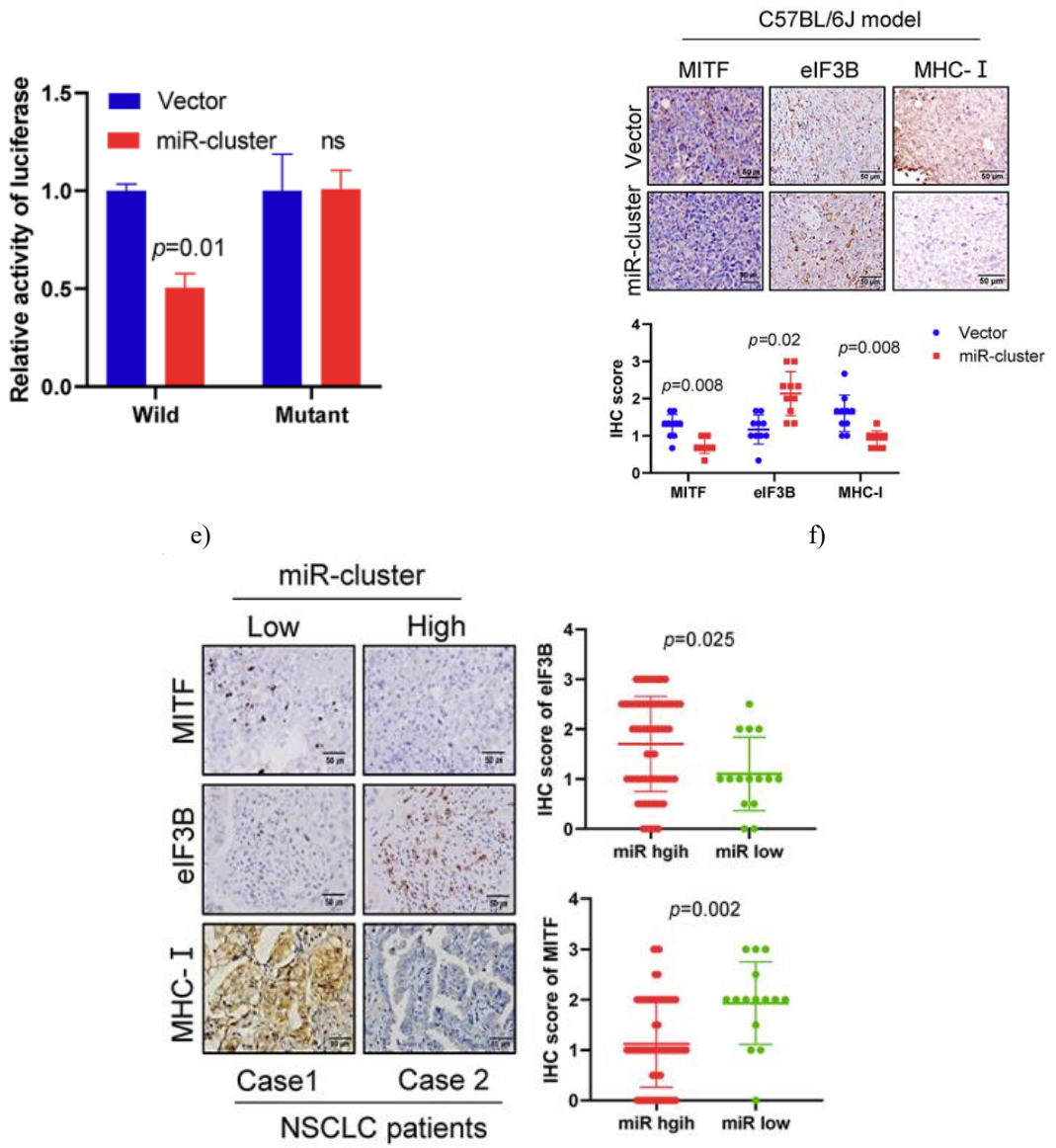

Figure 5. The miR-23a/27a/24−2 cluster diminishes MHC-I via the MITF/eIF3B pathway in NSCLC. (a) Sequence alignments indicating interactions between cluster miRNAs and MITF 3′-UTR. (b) Western blots revealing cluster overexpression reduce MITF and MHC-I while elevating eIF3B in NSCLC cells. (c) qRT-PCR confirming cluster-mediated MITF mRNA downregulation. (d) Western blots showing that MITF overexpression or eIF3B silencing reverses cluster-induced MHC-I loss in H1299 cells. Cells were transfected with specified plasmids and analyzed 72 hours post-transfection. Assays performed in triplicate (b-d). (e) Luciferase reporters demonstrating cluster suppression of wild-type but not mutant MITF 3′-UTR activity in NSCLC cells. (f) Representative IHC staining and scores for MITF, eIF3B, and MHC-I in C57BL/6J xenografts from **Figure 2d** (scale bar: 50 μm). (g) Representative IHC images and scores for MITF, eIF3B, and MHC-I in patient tumors with high (n = 67) or low (n = 15) cluster levels (scale bar: 50 μm). Results presented as mean ± SD. Significance by t-test (c and d), Wilcoxon signed-rank test (f), and Wilcoxon rank-sum test (g). miR-cluster, miR-23a/27a/24−2 cluster; miR high, high miR-23a/27a/24−2 cluster miRNA expression; miR low, low miR-23a/27a/24−2 cluster miRNA expression.

miRNAs in the miR-23a/27a/24−2 Cluster Sustain Their Levels via the β-catenin/TCF4 Pathway in NSCLC

To explore the upstream regulation of the miR-23a/27a/24−2 cluster in NSCLC, potential transcription factors were evaluated, identifying TCF4 as capable of binding the cluster promoter **(Figure 6a).** TCF4 serves as a downstream component of Wnt/β-catenin signaling and can influence miRNA transcription by occupying promoter regions [24]. Furthermore, our earlier work demonstrated that this cluster activates Wnt/β-catenin signaling, thereby enhancing TCF/LEF-driven gene transcription in NSCLC [9]. Accordingly, we hypothesized a positive feedback loop whereby the cluster perpetuates its own expression through β-catenin/TCF4. To validate this, TCF4's role was first assessed. Enforced TCF4 expression markedly elevated miR-23a, miR-27a, and miR-24-2 levels **(Figure 6b)** and boosted promoter-driven luciferase activity **(Figure 6c).** EMSA further showed direct TCF4 binding to the cluster promoter harboring consensus sites, with binding markedly weakened upon site mutation **(Figures 6d and 5f).** These data establish that TCF4 drives cluster miRNA transcription via promoter interaction. Subsequently, β-catenin's contribution to TCF4-dependent regulation was examined. β-catenin overexpression strengthened TCF4 recruitment to the promoter **(Figures 6e, f and 5g),** augmented promoter luciferase activity **(Figure 6g),** and increased cluster miRNA abundance **(Figure 6h).** Disruption of β-catenin–TCF4 binding using the inhibitor LF3 substantially blocked β-catenin-mediated cluster induction **(Figure 6i).** Overall, these results demonstrate that the miR-23a/27a/24−2 cluster autoregulates its expression via the β-catenin/TCF4 pathway in NSCLC.

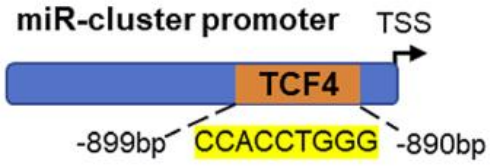

a)

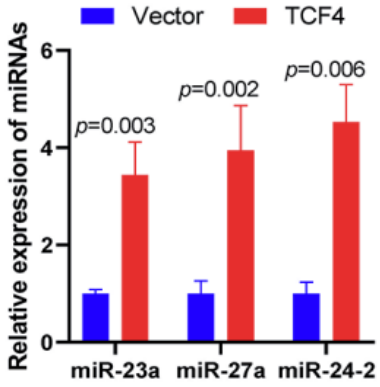

b)

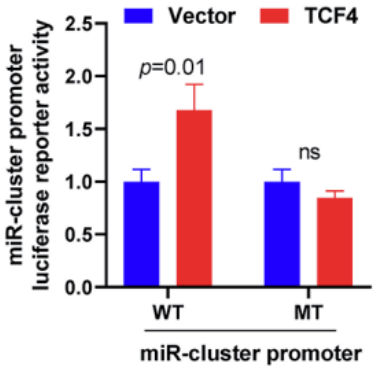

c)

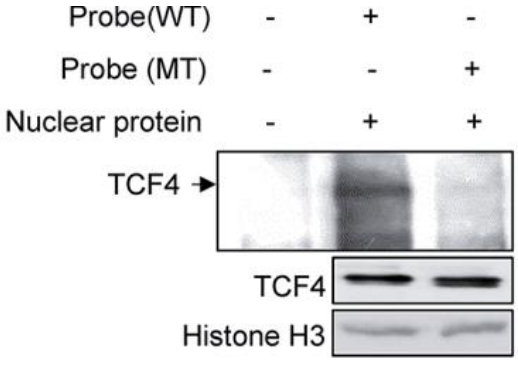

d)

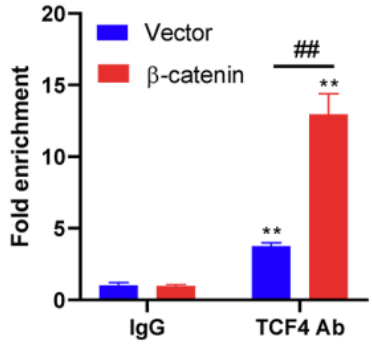

e)

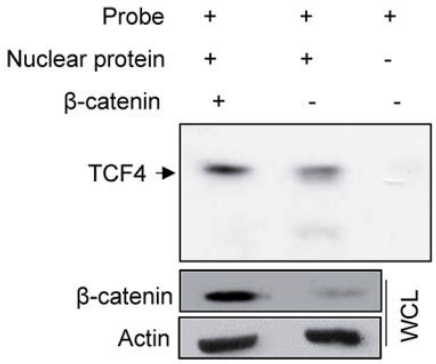

f)

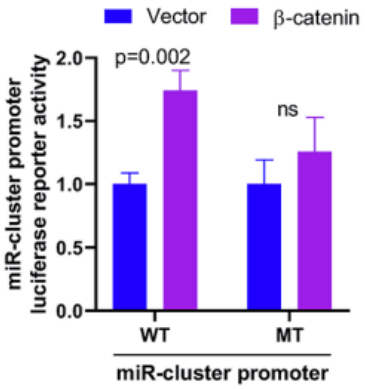

g)

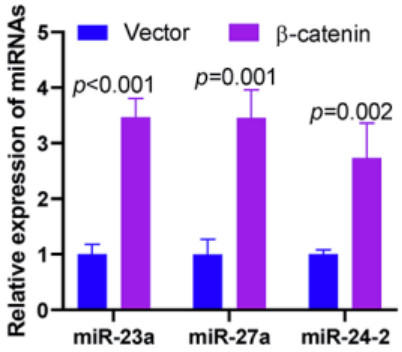

h)

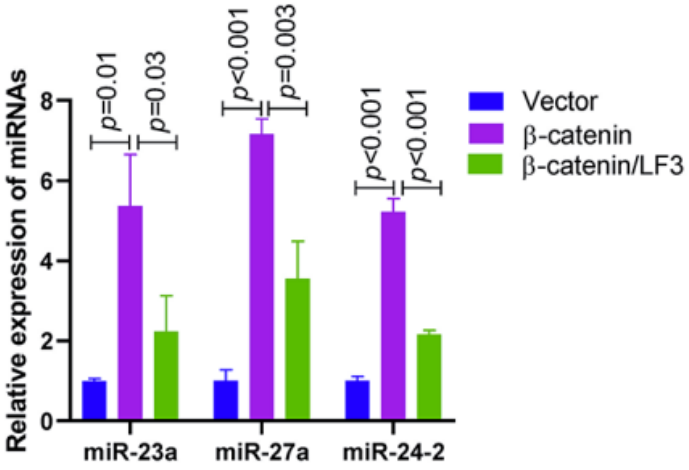

i)

Figure 6. The miR-23a/27a/24−2 cluster sustains its expression through the β-catenin/TCF4 pathway in NSCLC. (a) Predicted TCF4-binding motifs in the miR-23a/27a/24−2 cluster promoter region. (b) qRT-PCR revealing TCF4 overexpression elevates all cluster miRNAs in 293T cells. (c) Luciferase assays indicate that TCF4 enhances activity from the wild-type cluster promoter in 293T cells. (d) EMSA confirming TCF4 binding to the cluster promoter in 293T cells. (e) ChIP-qPCR demonstrating β-catenin overexpression augments TCF4 occupancy on the cluster promoter in 293T cells. **, $p < 0.01$ versus Vector (IgG); ##, $p < 0.01$ versus Vector (TCF4 Ab). (f) EMSA illustrating enhanced TCF4–promoter interaction upon β-catenin overexpression in 293T cells. (g) Luciferase assays showing β-catenin boosts wild-type but not mutant cluster promoter activity in 293T cells. (h) qRT-PCR confirming β-catenin overexpression raises cluster miRNA levels. (i) qRT-PCR indicating

that 30 μM LF3 treatment (6 hours) abrogates β-catenin-driven cluster miRNA induction in 293T cells. Cells were transfected with specified plasmids for 72 hours prior to assays (B-H). Values are mean ± SD. Significance by t-test (b, c, g, h) or one-way ANOVA with Duncan's test (e, i). miR-cluster, miR-23a/27a/24−2 cluster; ns, no significance; WT, wild type; MT, mutant; WCL, whole cell lysate.

Inhibition of the eIF3B axis markedly improves PD-1/PD-L1 blockade outcomes in lung tumors overexpressing the miR-23a/27a/24−2 Cluster

Since the miR-23a/27a/24−2 cluster controls critical determinants of PD-1/PD-L1 inhibitor response, we evaluated its impact on treatment resistance. Consistent with expectations, enforced cluster expression diminished tumor responsiveness to anti-PD-L1 monoclonal antibody **(Figure 7a)** and reduced CD8+ T cell tumor infiltration in LLC-derived C57BL/6J xenografts **(Figure 7b).**

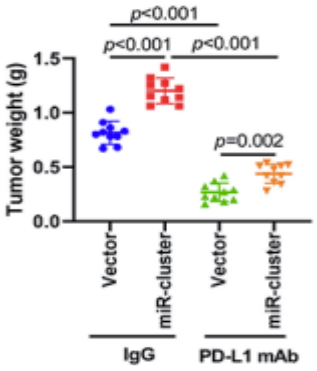

a)

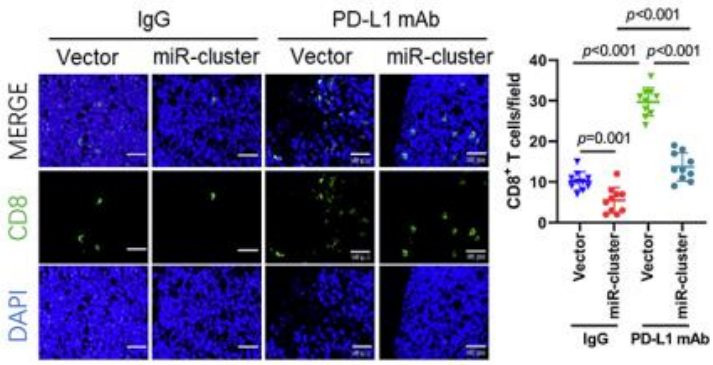

b)

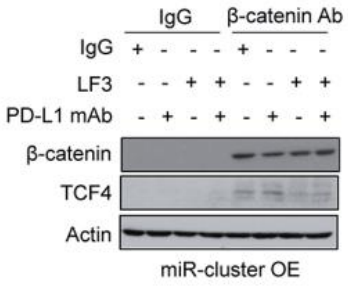

c)

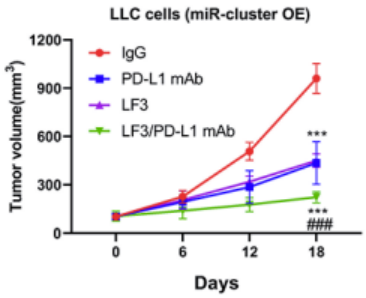

d)

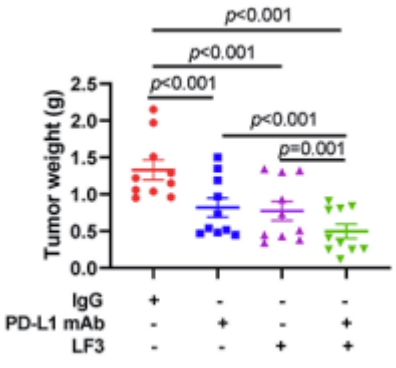

e)

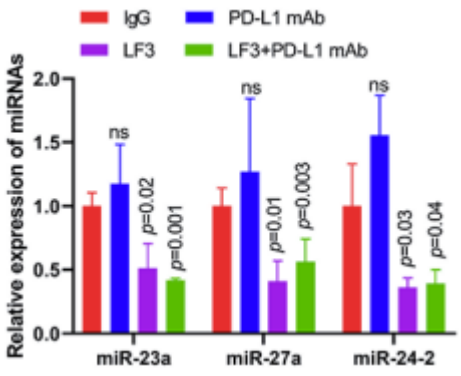

f)

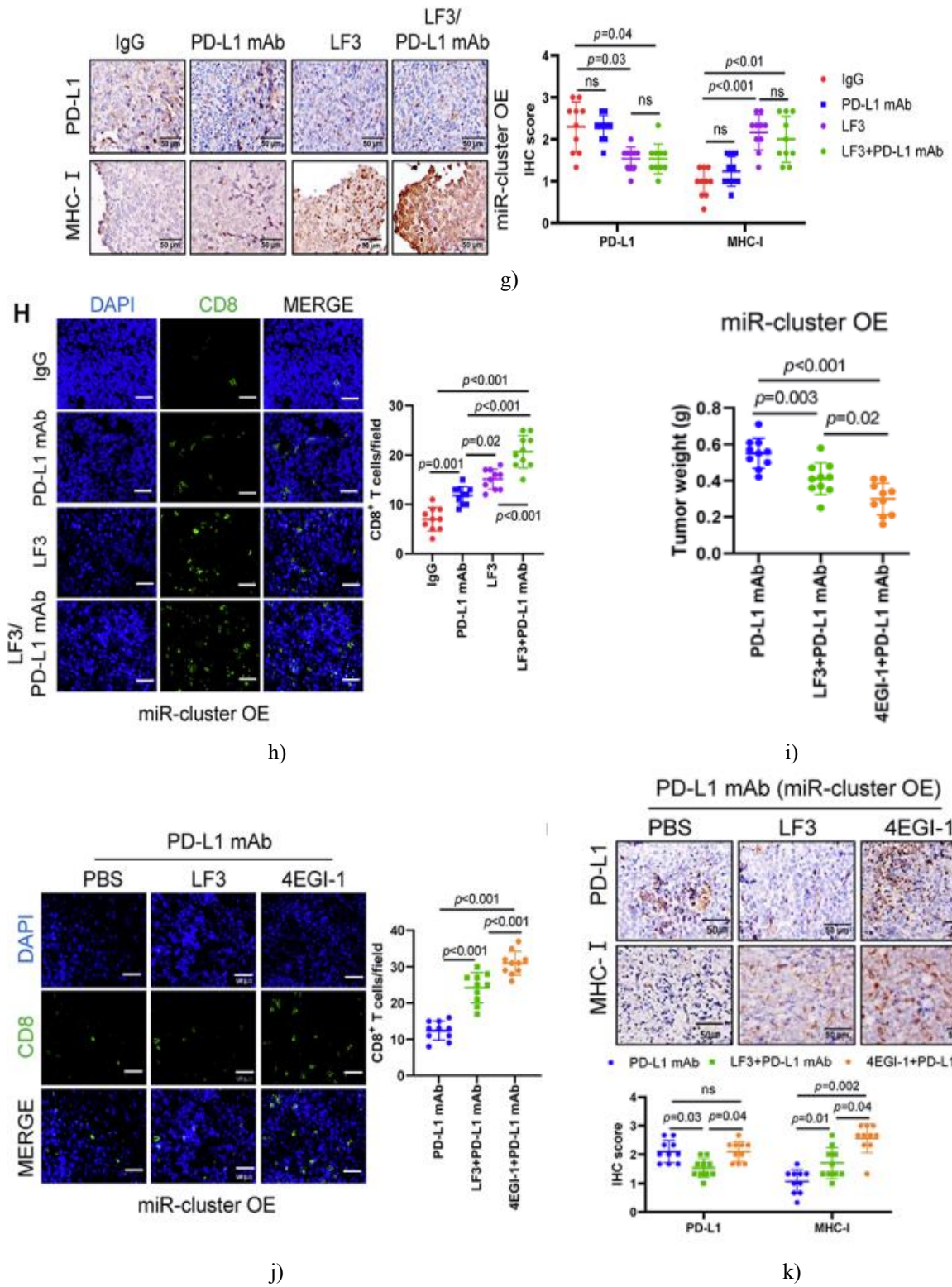

Figure 7. Enforced expression of the miR-23a/27a/24−2 cluster promotes resistance to PD-1/PD-L1 inhibition in LLC-derived C57BL/6J xenografts, while eIF3B targeting reverses cluster-mediated immune checkpoint blockade (ICB) resistance. (a) Final tumor weights from vector-control or cluster-overexpressing LLC xenografts in C57BL/6J mice administered IgG or anti-PD-L1 mAb. (b) Representative immunofluorescence staining for CD8+ T cells and quantification of infiltrates (100 × 100 μm field; scale bar: 50 μm) in tumors from (a). (c) Co-

immunoprecipitation demonstrating LF3 markedly disrupts β-catenin–TCF4 binding in xenograft tumors from (d). (d) Tumor growth curves, (e) final tumor weights, and (f) cluster miRNA levels in high-expressing LLC xenografts treated with indicated agents. Models were established with cluster-overexpressing LLC cells; therapy was initiated when the average volume reached ~100 mm³, comprising IgG, anti-PD-L1 mAb, LF3, or their combination. (g) Representative IHC staining and scores for PD-L1 and MHC-I across treatment groups in tumors from (d) (scale bar: 50 μm). (h) Representative immunofluorescence for CD8+ T cells and infiltrate counts (100 × 100 μm field) in tumors from (d) (scale bar: 50 μm). (i) Tumor weights, (j) representative immunofluorescence for CD8+ T cells (scale bar: 50 μm) with infiltrate quantification (100 × 100 μm field), and (k) representative IHC (scale bar: 50 μm) with scores for PD-L1 and MHC-I in high-cluster xenografts under specified treatments. Tumors were harvested 18 days post-treatment initiation for analyses (c-k). Each experimental arm included 10 animals. Values are mean ± SD. Significance assessed by one-way ANOVA with Duncan's test (a, b, d, e, f, h, i, j) or Kruskal-Wallis with Dunn's test (g, k). miR-cluster, miR-23a/27a/24−2 cluster; miR-cluster OE, miR-23a/27a/24−2 cluster overexpression; PD-L1 mAb, PD-L1 monoclonal antibody; ***, $p < 0.001$ versus IgG; ###, $p < 0.001$ versus monotherapy.

Prior reports have established that Wnt/β-catenin pathway activation [25] and the eIF3B/MHC-I axis [23] drive resistance to PD-1/PD-L1 inhibitors in malignancies. Considering that elevated miR-23a/27a/24−2 cluster levels foster such resistance in NSCLC, and that the cluster sustains itself via β-catenin/TCF4 while suppressing MHC-I through eIF3B, we assessed whether pharmacological interruption of these pathways could potentiate PD-1/PD-L1 blockade in cluster-high lung tumors. In vivo data showed that LF3-mediated disruption of β-catenin–TCF4 binding **(Figures 7c and 5h)** substantially retarded growth of cluster-overexpressing tumors relative to controls **(Figures 7d-e and 4e).** Strikingly, combining LF3 with anti-PD-L1 mAb yielded superior tumor suppression compared to either agent alone **(Figures 7d-e).** LF3 also reduced cluster miRNA abundance **(Figure 7f),** lowered PD-L1, and restored MHC-I **(Figure 7g).** The dual regimen most effectively boosted CD8+ T cell tumor infiltration **(Figure 7h).** To contrast pathway targeting, we employed 4EGI-1, which blocks eIF3B incorporation into the translation initiation complex and inhibits the MITF/eIF3B cascade [23, 26]. Results indicated that eIF3B inhibition with 4EGI-1 more potently augmented anti-PD-L1 efficacy than β-catenin/TCF4 blockade with LF3 in cluster-high tumors **(Figure 7i).** Combined 4EGI-1 and anti-PD-L1 markedly enhanced CD8+ T cell infiltration **(Figure 7j)** and upregulated MHC-I without reversing cluster-driven PD-L1 elevation **(Figure 7k).** Collectively, these findings demonstrate that eIF3B targeting substantially improves PD-1/PD-L1 blockade outcomes in lung cancers overexpressing the miR-23a/27a/24−2 cluster.

This investigation explored the underlying mechanisms through which the miR-23a/27a/24−2 cluster miRNAs facilitate immune escape and resistance to PD-1/PD-L1 inhibition in NSCLC. Substantial evidence highlights PD-L1 [27] and MHC-I [28] as pivotal regulators of antitumor immunity. PD-L1, displayed on tumor cell surfaces, suppresses T cell activity via interaction with PD-1, representing a major route for malignant cells to evade detection. Similarly, reduced MHC-I levels constitute another critical escape strategy. MHC-I presents peptide antigens to the immune system, enabling recognition and destruction of aberrant cells [29]. When these antigens are tumor-derived, CD8+ T cells become activated upon binding, triggering cytotoxic elimination of malignant cells [29]. Regrettably, MHC-I deficiency or loss occurs commonly across cancers, including lung carcinoma [30, 31], impairing T cell surveillance and permitting tumor persistence [31]. Here, we established that elevated miR-23a/27a/24−2 cluster levels drive NSCLC immune evasion and PD-1/PD-L1 blockade insensitivity. Mechanistically, the cluster induced PD-L1 by repressing its negative regulator CBLB and suppressed MHC-I via eIF3B induction through direct MITF inhibition. Comparable immunosuppressive roles for these miRNAs have emerged in other malignancies. For instance, miR-27a was shown to diminish MHC-I and CD8+ T cell infiltration in colorectal tumors [28]. Lin and colleagues found miR-23a elevated in cytotoxic CD8+ T cells, with its inhibition countering tumor-mediated immunosuppression in lung carcinoma [32]. Furthermore, heightened miR-23a and miR-27a in macrophages promoted PD-L1 via PTEN/PIK3 signaling, aiding evasion in hepatocellular [33] and breast [34] cancers. Altogether, these observations

reinforce that cluster overexpression fosters immune avoidance through PD-L1 elevation and MHC-I reduction, uncovering a previously undescribed regulatory pathway in NSCLC.

We also clarified how the miR-23a/27a/24−2 cluster sustains its elevated abundance in NSCLC. Aberrant upregulation affects roughly 50% of early-stage cases and strongly predicts progression [9], yet the basis remained elusive. Our findings showed that TCF4 directly occupies the cluster promoter to enhance transcription, with this process augmented by β-catenin. Notably, prior work from our group indicated the cluster boosts TCF/LEF-dependent transcription by activating Wnt/β-catenin through suppression of pathway inhibitors in NSCLC [9]. Thus, a self-reinforcing loop emerges wherein the cluster perpetuates its levels via β-catenin/TCF4 activation. Disrupting this circuit could offer therapeutic promise for cluster-high NSCLC. Indeed, earlier results demonstrated that cluster knockdown or β-catenin silencing curbs tumor advancement in such contexts [9].

Lastly, we introduce an innovative approach for managing cluster-high NSCLC. The cluster stimulates both β-catenin signaling [9] and the eIF3B cascade, each implicated in PD-1/PD-L1 resistance [23, 35]. We confirmed that interfering with either β-catenin/TCF4 or eIF3B markedly potentiates anti-PD-L1 responses, though eIF3B blockade proved superior. This disparity likely stems from distinct impacts on PD-L1 versus MHC-I. Clinical outcomes with PD-1/PD-L1 agents correlate tightly with tumoral PD-L1 abundance [36, 37], and its forced elevation can improve treatment success [38]. Our experiments indicated β-catenin/TCF4 inhibition restores MHC-I but lowers PD-L1, whereas eIF3B targeting preserves cluster-driven PD-L1 elevation while robustly recovering MHC-I.

Conclusion

Overall, the miR-23a/27a/24−2 cluster sustains its abundance via β-catenin/TCF4 pathway activation in NSCLC. Elevated cluster levels boost PD-L1 through CBLB repression and diminish MHC-I by inducing eIF3B via MITF targeting (**Figure 8**b). Moreover, this work outlines a treatment paradigm whereby eIF3B inhibition substantially augments PD-1/PD-L1 blockade effectiveness in cluster-overexpressing lung tumors, achieved by MHC-I restoration alongside retention of cluster-induced PD-L1 elevation (**Figure 8a**).

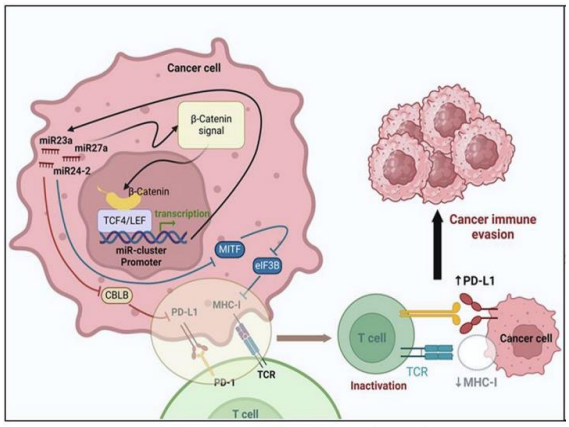

a)

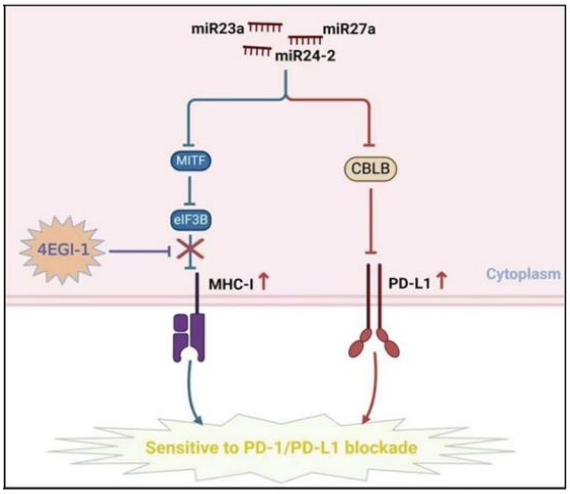

b)

Figure 8. Schematic models depicting how miR-23a/27a/24−2 cluster miRNAs autoregulate and drive immune escape (a), and how eIF3B targeting renders cluster-high tumors susceptible to PD-1/PD-L1 inhibition (b).

Acknowledgments: None

Conflict of Interest: None

Financial Support: This work was supported by the National Natural Science Foundation of China (81672283, to H.J.), the Chongqing Natural Science Foundation (cstc2021jcyj-msxmX0350, to H.J.), and the Beijing Natural Science Foundation (7232168, to R.-T.W.).

Ethics Statement: This study was approved by the Ethics Committee of Daping Hospital of Army Medical University (Medical Research Ethics Review No.120), and all patients obtained informed consent before enrollment. All mouse procedures were approved by the Laboratory Animal Welfare and Ethics Committee of Army Medical University (AMUWEC20211547).

References

1. Bray F, Laversanne M, Sung HYA, Ferlay J, Siegel RL, Soerjomataram I, Jemal A. Global cancer statistics 2022: GLOBOCAN estimates of incidence and mortality worldwide for 36 cancers in 185 countries. Ca-Cancer J Clin. 2024;74(3):229–63.
2. Cronin KA, Lake AJ, Scott S, Sherman RL, Noone AM, Howlader N, Henley SJ, Anderson RN, Firth AU, Ma JM et al. Annual Report to the Nation on the Status of Cancer, part I: National cancer statistics. Cancer-Am Cancer Soc. 2018;124(13):2785–2800.
3. Zavitsanou AM, Pillai R, Hao Y, Wu WL, Bartnicki E, Karakousi T, Rajalingam S, Herrera A, Karatza A, Rashidfarrokhi A, et al. KEAP1 mutation in lung adenocarcinoma promotes immune evasion and immunotherapy resistance. Cell Rep. 2023;42(11):113295.
4. Vinay DS, Ryan EP, Pawelec G, Talib WH, Stagg J, Elkord E, Lichtor T, Decker WK, Whelan RL, Kumara HMCS, et al. Immune evasion in cancer: mechanistic basis and therapeutic strategies. Semin Cancer Biol. 2015;35:S185–98.
5. Cable J, Greenbaum B, Pe'er D, Bollard CM, Bruni S, Griffin ME, Allison JP, Wu CJ, Subudhi SK, Mardis ER et al. Frontiers in cancer immunotherapy-a symposium report. Ann Ny Acad Sci: 2021, 1489(1):30–47.
6. Sharma P, Hu-Lieskovan S, Wargo JA, Ribas A. Primary, adaptive, and Acquired Resistance to Cancer Immunotherapy. Cell. 2017;168(4):707–23.
7. Cioffi M, Trabulo SM, Vallespinos M, Raj D, Kheir TB, Lin ML, Begum J, Baker AM, Amgheib A, Saif J et al. The miR-25-93-106b cluster regulates tumor metastasis and immune evasion via modulation of CXCL12 and PD-L1. Oncotarget. 2017;8(13):21609–21625.
8. Kundu ST, Rodriguez BL, Gibson LA, Warner AN, Perez MG, Bajaj R, Fradette JJ, Class CA, Solis LM, Alvarez FRR, et al. The microRNA-183/96/182 cluster inhibits lung cancer progression and metastasis by inducing an interleukin-2-mediated antitumor CD8 cytotoxic T-cell response. Gene Dev. 2022;36(9–10):582–600.
9. Fan XQ, Tao SL, Li Q, Deng B, Tan QY, Jin H. The miR-23a/27a/24 – 2 cluster promotes postoperative progression of early-stage non-small cell lung cancer. Mol Ther-Oncolytics. 2022;24:205–17.
10. Muto S, Enta A, Maruya Y, Inomata S, Yamaguchi H, Mine H, Takagi H, Ozaki Y, Watanabe M, Inoue T, et al. Wnt/β-Catenin signaling and resistance to Immune Checkpoint inhibitors: from non-small-cell lung Cancer to other cancers. Biomedicines. 2023;11(1):190.
11. Chandran PA, Keller A, Weinmann L, Seida AA, Braun M, Andreev K, Fischer B, Horn E, Schwinn S, Junker M, et al. The TGF-β-inducible miR-23a cluster attenuates IFN-γ levels and antigen-specific cytotoxicity in human CD8 T cells. J Leukoc Biol. 2014;96(4):633–45.
12. Li Q, Zhou ZW, Lu J, Luo H, Wang SN, Peng Y, Deng MS, Song GB, Wang JM, Wei X, et al. PD-L1P146R is prognostic and a negative predictor of response to immunotherapy in gastric cancer. Mol Ther. 2022;30(2):621–31.
13. Shang S, Yang YW, Chen F, Yu L, Shen SH, Li K, Cui B, Lv XX, Zhang C, Yang C, et al. TRIB3 reduces CD8 T cell infiltration and induces immune evasion by repressing the STAT1-CXCL10 axis in colorectal cancer. Sci Transl Med. 2022;14(626):eabf0992.
14. Li Q, Zhou ZW, Duan W, Qian CY, Wang SN, Deng MS, Zi D, Wang JM, Mao CY, Song GB, et al. Inhibiting the redox function of APE1 suppresses cervical cancer metastasis via disengagement of ZEB1 from E-cadherin in EMT. J Exp Clin Canc Res. 2021;40(1):220.
15. Nuovo GJ. In situ detection of microRNAs in paraffin embedded, Formalin fixed tissues and the co-localization of their putative targets. Methods. 2010;52(4):307–15.
16. Guo ZY, Hardin H, Montemayor-Garcia C, Asioli S, Righi A, Maletta F, Sapino A, Lloyd RV. In situ hybridization analysis of miR-146b-5p and miR-21 in thyroid nodules: diagnostic implications. Endocr Pathol. 2015;26(2):157–63.
17. Li JW, Jiang HM, Lv ZY, Sun ZY, Cheng CQ, Tan GH, Wang MC, Liu AL, Sun H, Guo H, et al. Articular fibrocartilage-targeted therapy by

microtubule stabilization. Sci Adv. 2022;8(46):eabn8420.
18. Dai FQ, Li CR, Fan XQ, Tan L, Wang RT, Jin H. Mir-150-5p inhibits non-small-cell Lung Cancer Metastasis and recurrence by targeting HMGA2 and β-Catenin signaling. Mol Ther-Nucl Acids. 2019;16:675–85.
19. Zhang Q, Liu W, Zhang HM, Xie GY, Miao YR, Xia MX, Guo AY. hTFtarget: a comprehensive database for regulations of human transcription factors and their targets. Genom Proteom Bioinf. 2020;18(2):120–8.
20. Vlachos IS, Zagganas K, Paraskevopoulou MD, Georgakilas G, Karagkouni D, Vergoulis T, Dalamagas T, Hatzigeorgiou AG. DIANA-miRPath v3.0: deciphering microRNA function with experimental support. Nucleic Acids Res. 2015;43(W1):W460–6.
21. Liu ZC, Wang TT, She YL, Wu KQ, Gu SR, Li L, Dong CL, Chen C, Zhou YX. N-methyladenosine-modified circIGF2BP3 inhibits CD8 T-cell responses to facilitate tumor immune evasion by promoting the deubiquitination of PD-L1 in non-small cell lung cancer. Mol Cancer. 2021;20(1):105.
22. Wang S, Xu L, Che XF, Li C, Xu L, Hou KZ, Fan YB, Wen T, Qu XJ, Liu YP. E3 ubiquitin ligases Cbl-b and c-Cbl downregulate PD-L1 in wild-type non-small cell lung cancer. Febs Lett. 2018;592(4):621–30.
23. Santasusagna S, Zhu S, Jawalagatti V, Carceles-Cordon M, Ertel A, Garcia-Longarte S, Song WM, Fujiwara N, Li P, Mendizabal I, et al. Master transcription factor reprogramming unleashes selective translation promoting Castration Resistance and Immune Evasion in Lethal prostate Cancer. Cancer Discov. 2023;13(12):2584–609.
24. Rambow F, Bechadergue A, Luciani F, Gros G, Domingues M, Bonaventure J, Meurice G, Marine JC, Larue L. Regulation of Melanoma Progression through the TCF4/miR-125b/NEDD9 Cascade. J Invest Dermatol. 2016;136(6):1229–37.
25. de Galarreta MR, Bresnahan E, Molina-Sánchez P, Lindblad KE, Maier B, Sia D, Puigvehi M, Miguela V, Casanova-Acebes M, Dhainaut M, et al. β-Catenin activation promotes Immune escape and resistance to Anti-PD-1 therapy in Hepatocellular Carcinoma. Cancer Discov. 2019;9(8):1124–41.
26. Moerke NJ, Aktas H, Chen H, Cantel S, Reibarkh MY, Fahmy A, Gross JD, Degterev A, Yuan JY, Chorev M, et al. Small-molecule inhibition of the interaction between the translation initiation factors eIF4E and eIF4G. Cell. 2007;128(2):257–67.
27. Wang J, Ge JS, Wang YA, Xiong F, Guo JY, Jiang XJ, Zhang LS, Deng XY, Gong ZJ, Zhang SS, et al. EBV miRNAs BART11 and BART17-3p promote immune escape through the enhancer-mediated transcription of PD-L1. Nat Commun. 2022;13(1):866.
28. Colangelo T, Polcaro G, Ziccardi P, Pucci B, Muccillo L, Galgani M, Fucci A, Milone MR, Budillon A, Santopaolo M, et al. Proteomic screening identifies calreticulin as a miR-27a direct target repressing MHC class I cell surface exposure in colorectal cancer. Cell Death Dis. 2016;7(2):e2120.
29. Wu XY, Li TH, Jiang R, Yang X, Guo HQ, Yang R. Targeting MHC-I molecules for cancer: function, mechanism, and therapeutic prospects. Mol Cancer. 2023;22(1):194.
30. Korkolopoulou P, Kaklamanis L, Pezzella F, Harris AL, Gatter KC. Loss of antigen-presenting molecules (MHC class I and TAP-1) in lung cancer. Brit J Cancer. 1996;73(2):148–53.
31. .Dhatchinamoorthy K, Colbert JD, Rock KL. Cancer Immune Evasion through loss of MHC Class I Antigen Presentation. Front Immunol. 2021;12:636568.
32. Lin R, Chen L, Chen G, Hu CY, Jiang S, Sevilla J, Wan Y, Sampson JH, Zhu B, Li QJ. Targeting miR-23a in CD8 cytotoxic T lymphocytes prevents tumor-dependent immunosuppression. J Clin Invest. 2014;124(12):5352–67.
33. Liu JT, Fan LL, Yu HQ, Zhang J, He Y, Feng DC, Wang F, Li XQ, Liu QQ, Li YH, et al. Endoplasmic reticulum stress causes Liver Cancer cells to Release Exosomal miR-23a-3p and Up-regulate programmed death Ligand 1 expression in macrophages. Hepatology. 2019;70(1):241–58.
34. Yao XL, Tu Y, Xu YL, Guo YY, Yao F, Zhang XH. Endoplasmic reticulum stress-induced exosomal miR-27a-3p promotes immune escape in breast cancer via regulating PD-L1 expression in macrophages. J Cell Mol Med. 2020;24(17):9560–73.
35. Luke JJ, Bao RY, Sweis RF, Spranger S, Gajewski TF. WNT/β-catenin pathway activation correlates with Immune Exclusion across Human cancers. Clin Cancer Res. 2019;25(10):3074–83.

36. Herbst RS, Soria JC, Kowanetz M, Fine GD, Hamid O, Gordon MS, Sosman JA, McDermott DF, Powderly JD, Gettinger SN, et al. Predictive correlates of response to the anti-PD-L1 antibody MPDL3280A in cancer patients. Nature. 2014;515(7528):563–7.
37. Iwai Y, Ishida M, Tanaka Y, Okazaki T, Honjo T, Minato N. Involvement of PD-L1 on tumor cells in the escape from host immune system and tumor immunotherapy by PD-L1 blockade. P Natl Acad Sci USA. 2002;99(19):12293–7.
38. Zhang JF, Bu X, Wang HZ, Zhu YS, Geng Y, Nihira NT, Tan YY, Ci YP, Wu F, Dai XP, et al. Cyclin D-CDK4 kinase destabilizes PD-L1 via cullin 3-SPOP to control cancer immune surveillance. Nature. 2018;553(7686):91–5.